Journal of King Saud University – Science 32 (2020) 2480–2488

Contents lists available at ScienceDirect

Journal of King Saud University – Science

journal homepage: www.sciencedirect.com

Original article

Apoptosis-inducing potential of biosynthesized silver nanoparticles in breast cancer cells

Ahmed Ali Al-kawmani [a], Khalid Mashai Alanazi [a], Mohammad Abul Farah [a,*], M. Ajmal Ali [b], Waleed Ali Qaid Hailan [a], Fahad M.A. Al-Hemaid [b]

[a] Department of Zoology, College of Science, King Saud University, Riyadh 11451, Saudi Arabia
[b] Department of Botany and Microbiology, College of Science, King Saud University, Riyadh 11451, Saudi Arabia

ARTICLE INFO

Article history:
Received 23 January 2020
Revised 9 March 2020
Accepted 3 April 2020
Available online 13 April 2020

Keywords:
Ochradenus arabicus
Silver nanoparticles
Apoptosis
Autophagy
Reactive oxygen species
Cytotoxicity

ABSTRACT

Objectives: Silver nanoparticles (AgNPs) are one of the most vital and fascinating nanomaterials used in biomedical applications. Moreover, natural products from medicinal plants provide unlimited opportunities for drug development owing to the unmatched availability of a biochemical diversity. In this study, we biosynthesized AgNPs from the leaf extract of *Ochradenus arabicus* using silver nitrate and evaluated the cytotoxicity and apoptosis inducing ability of the *O. arabicus* AgNPs (OA-synthesized AgNPs) against the MCF-7 human breast cancer cells.
Methods: The OA-synthesized AgNPs were characterized by X-ray diffraction, UV–visible spectroscopy, and transmission electron microscopy.
Results: The OA-synthesized AgNPs were highly toxic to the MCF-7 cells as the cell proliferation was significantly decreased post-treatment. The intracellular level of reactive oxygen species (ROS) was significantly increased ($p < 0.05$). Moreover, a dose-dependent increase in the percentage of apoptosis and autophagy was also evident.
Conclusion: The findings of this study confirm the ability of OA-synthesized AgNPs to stimulate apoptosis and suppress cell growth and proliferation.

1. Introduction

Breast cancer, a malignant tumor, is the second most globally encountered cancer and a leading cause of cancer-related deaths among females in the developing nations (Jemal et al., 2011). The conventional treatment methods for breast cancer lead to unwanted side effects and resistance to anticancer drugs (Lodha et al., 2011). Therefore, there is a need for developing effective novel therapies using natural products as anticancer agents for decreasing the incidence and severity of breast cancer (Arulvasu et al., 2010). Medicinal plants have shown activity against various metabolic diseases and cancers. In recent years, nanoparticles (NPs) synthesized from medicinal plants have become the focus of research (Kuppusamy et al., 2016). NPs play a critical role in refining the compatibility and bioavailability of natural products in the treatment of several chronic diseases, including cancer (Rao et al., 2016).

The increasing production and use of nanomaterials have led to the emergence of new materials, which contribute to the environmental burden of engineered NPs. The release of the NPs in the environment has become a human health concern (Ribeiro et al., 2013). Metal NPs are produced in different ways, most commonly by chemical and physical methods. Through these methods, pure NPs are produced; however, the chemicals used in the synthesis process can be toxic and expensive, and the process consumes a lot of energy. Thus, these methods are not suitable for biological applications (Ghaffari-Moghaddam et al., 2014).

Many experimental challenges and issues are encountered while assessing the toxicity of nanomaterials; hence, further studies will be needed to conclusively establish the safety/toxicity of NPs. The main molecular mechanism of toxicity is induction of oxidative stress through the production of free radicals. Reactive oxygen species (ROS) are important molecules that induce apoptosis, DNA damage, oxidative stress-induced damage, and many

* Corresponding author.
E-mail address: mfarah@ksu.edu.sa (M.A. Farah).
Peer review under responsibility of King Saud University.

Production and hosting by Elsevier

https://doi.org/10.1016/j.jksus.2020.04.002
1018-3647/

other cellular processes. Excessive free radicals damage biological components through oxidation of lipids, proteins, and DNA (Nel et al., 2006; Deavall et al., 2012). One of the most important impacts of the action of NPs seems to be their ability to cause DNA damage. DNA damage is usually detrimental with adverse consequences on metabolism and cell cycle, and can be lethal (Rodriguez-Rocha et al., 2011).

Recently, extracts of *Adenium obesum* have been successfully used to prepare NPs and their cytotoxicity against MCF-7 cells has been reported (Farah et al., 2016). However, the mechanisms of apoptosis and DNA damage induced by plant extract-based nanomaterials are unclear. *Ochradenus arabicus* is a medicinal plant belonging to the family *Resedaceae* that is mostly grown in the desert regions of middle-east countries, including Saudi Arabia (Miller, 1984). The biological activity of *O. arabicus* is unknown as is its potential as a source of silver NPs (AgNPs). The present investigation was undertaken to develop a novel method for the biosynthesis of *O. arabicus* AgNPs (OA-synthesized AgNPs) using *O. arabicus* leaves extract. The NPs were characterized by standard methods and their potential to induce ROS and cell death in breast cancer cells was evaluated.

2. Materials and methods

2.1. Plant material and preparation of extract

The leaves of *O. arabicus* (Fig. 1A) were collected from a natural habitat around Riyadh, Saudi Arabia. The crude aqueous extract was prepared by a method reported previously (Farah et al., 2016). Briefly, leaves were washed thoroughly and crushed into small pieces, oven-dried at 50 °C, and powdered. The dried and powdered leaves were boiled in deionized water for 10 min. After the solution was cooled, the aqueous extract was filtered through the Whatman filter paper No. 1 (Maidstone, UK).

2.2. Biosynthesis and characterization of AgNPs

AgNPs were biosynthesized by a method developed in our laboratory and reported previously (Farah et al., 2016). In brief, a reaction mixture containing 99 mL of 1 mM $AgNO_3$ + 1 mL of aqueous leaves extract was prepared and incubated at 25 °C until the slight yellowish solution turned brown, which was indicative of the synthesis of AgNPs. Finally, the AgNPs were recovered by centrifuging the reaction mixture at 10,000 rpm for 10 min and dissolving the pellet in sterile distilled water. The biosynthesized AgNPs were stored under ambient conditions for further characterization and application. The color change was monitored by scanning the sample with an ultraviolet–visible (US–vis) spectrophotometer (BioTek, Winooski, VA, USA) at 300 nm–700 nm for up to 120 min. The crystalline structure of the biosynthesized AgNPs was investigated by recording their X-ray diffraction (XRD) pattern in a scanning mode using an X'pert Pro diffract meter (PANalytical, Almelo, Netherlands). To confirm their size and shape, transmission electron microscopy (TEM) images of the AgNPs were captured after dispersing the sample on a carbon-coated copper TEM grid.

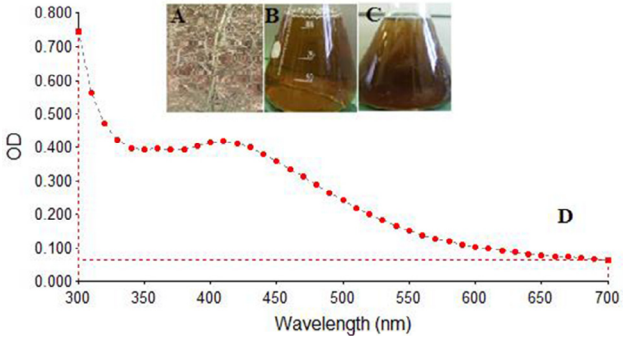

Fig. 1. Synthesis of *O. arabicus* silver nanoparticles (OA-synthesized AgNPs). (A) Dried leaves of *O. arabicus*. (B) Mixture of 1 mM $AgNO_3$ solution and *O. arabicus* leaves extract. (C) Change in the color of the reaction solution from slight yellowish to brown after 120 min, indicating the green synthesis of OA-synthesized AgNPs. (D) UV–visible absorption spectra of the OA-synthesized AgNPs exhibited a strong broad peak at 420 nm.

2.3. Cell culture and cytotoxicity assay

MCF-7 breast cancer cells (American Type Culture Collection, Manassas, VA, USA) were cultured at 37 °C and 5% CO_2 in a minimum essential medium (MEM) supplemented with 1% penicillin/streptomycin and 10% FBS. The cells were grown as adherent monolayers and the exponentially growing MCF-7 cells were trypsinized and re-suspended in MEM at a density of 1×10^5 cells/mL and used for subsequent experiments. The cytotoxicity of OA-synthesized AgNPs was assessed by the MTT colorimetric assay (Mosmann, 1983) performed with some modifications. MCF-7 cells at a density of 10,000 cells/well were grown in 96-well plates and then treated with various concentrations of OA-synthesized AgNPs (600 μg/mL, 500 μg/mL, 400 μg/mL, 300 μg/mL, 200 μg/mL, 100 μg/mL, 50 μg/mL, 25 μg/mL, and 15 μg/mL) for 24 h. A CellTiter 96® non-radioactive cell proliferation assay kit (Promega, Madison, WI, USA) was used following the manufacturer's instructions. At the end of the experiment, the optical density (OD) of each well was recorded with a microplate reader (BioTek®, Winooski, VA, USA) at 550 nm. To determine the IC_{50} value, the percentage of cytotoxicity of the OA-synthesized AgNPs in the MCF-7 cells was compared to that in the untreated cells. Further, to analyze any changes in the morphology, MCF-7 cells were treated with three sub-lethal concentrations of OA-synthesized AgNPs (25 μg/mL, 50 μg/mL, and 75 μg/mL) for 24 h. The cells were observed under a phase contrast inverted microscope (Olympus, Tokyo, Japan) and images were captured at 100X magnification.

2.4. Intracellular ROS measurement

Intracellular generation of ROS was analyzed by spectrofluorometry and fluorescence microscopy. MCF-7 cells were grown and treated with 25 μg/mL, 50 μg/mL, and 75 μg/ml OA-synthesized AgNPs for 24 h at 37 °C. Then, the cells were stained with 25 μM working solution of DCFH-DA in a serum-free medium at 37 °C for 30 min. The microplate reader (BioTek®) was used to record the intensity of the green fluorescence (excitation wavelength, 485 nm; emission wavelength, 528 nm). Similarly, fluorescence images were acquired using appropriate filter settings in a compound microscope (BX41 Olympus, Tokyo, Japan) equipped with a fluorescence attachment.

2.5. Annexin-V apoptosis assay

Annexin V-FITC apoptosis detection kit (BD Biosciences, San Diego, USA) was used to measure apoptosis in the MCF-7 cells. Briefly, cells were cultured and treated with three sub-lethal doses of OA-synthesized AgNPs (25 μg/mL, 50 μg/mL, and 75 μg/mL) for 24 h. Next, the cells were re-suspended in 100 μL of 1X binding buffer (1×10^6 cells/mL). Then, 5 μL each of annexin V–FITC and PI were added to the cell suspension and the suspension was incubated in dark for 20 min at room temperature. Finally, the samples were analyzed in a BD FACS Calibur flow cytometer (BD, Miami, FL, USA).

2.6. Analysis of apoptosis induction by acridine orange–ethidium bromide staining

To detect condensed apoptotic or necrotic nuclei, MCF-7 cells were cultured and exposed to 25 μg/mL, 50 μg/mL, and 75 μg/mL OA-synthesized AgNPs as mentioned above. After 24 h of treatment, the cells were stained by adding equal volumes of acridine orange (AO) and ethidium bromide (20 μg/mL; each prepared in PBS). The stained cells were observed under a compound microscope (Olympus BX41, Japan) equipped with a fluorescence attachment. The images were captured using appropriate filter settings for fluorescence (excitation wavelength, 488 nm; emission wavelength, 525 nm). More than 300 cells were quantified to estimate the percentage of apoptotic and necrotic cells based on the uptake of AO and ethidium bromide. The criteria for identification were as follows: intact green nucleus, viable cells; dense green areas of chromatin condensation in the nucleus, apoptosis; intact orange nucleus, necrosis.

2.7. Detection of autophagy by acridine orange staining

The presence of acidic vesicular organelles (AVOs) in MCF-7 cells was considered as a marker of autophagy induction. The cells were cultured and exposed to the three sub-lethal concentrations of OA-synthesized AgNPs (25 μg/mL, 50 μg/mL, and 75 μg/mL) and further incubated for 24 h. Then, the cells were stained with 5 μg/mL AO in a serum free medium at room temperature. The stained cells were observed under a compound microscope (Olympus BX41, Japan) fitted with a fluorescence attachment. The images were captured using appropriate filter settings for fluorescence (excitation wavelength, 488 nm; emission wavelength, 525 nm).

2.8. Statistical analysis

All the above-mentioned experiments were performed independently in triplicate. The results of the three replicates have been presented as mean ± standard errors of the mean (SEM). The MTT assay data have been presented as linear graphs. The results were statistically analyzed by applying the Student's *t*-test for comparison between the means using a significance level of $p < 0.05$.

3. Results

3.1. Biosynthesis and characterization of AgNPs

After the aqueous leaves extract of *O. arabicus* was mixed with $AgNO_3$ solution, the color of the reaction mixture changed from yellowish to brown over a period of 120 min (Fig. 1B and 1C). This change in the color of the reaction mixture indicated that the *O. arabicus* extract accelerated the biosynthesis of the OA-synthesizedAgNPs, which was found to be consistent with results of the previous reports (Dwivedi and Gopal, 2010; Farah et al., 2016). The UV–vis spectroscopy of OA-synthesized AgNPs revealed a distinct peak at 420 nm (Fig. 1D). The UV–vis spectra recorded after 24 h of completion of biosynthesis reaction revealed increased absorption, confirming the completion of OA-synthesized AgNPs.

The crystalline structure of the synthesized AgNPs was investigated by XRD. The X-ray patterns of the synthesized and subsequently lyophilized AgNPs have been shown in Fig. 2B. The XRD peaks at 38.1° and 44.3° may be attributed to the (1 1 1 and 2 0 0) crystalline planes of the face-centered cubic structure of the AgNPs. TEM was used to examine the morphology and size of the biosynthesized OA-synthesized AgNPs. The OA-synthesized AgNPs

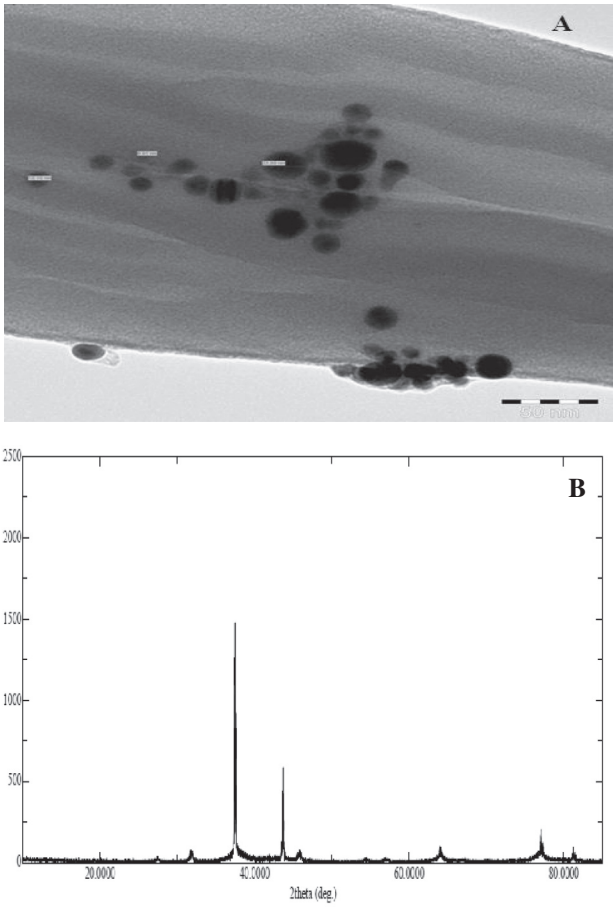

Fig. 2. (A) Representative images of transmission electron microscopy (TEM). The images revealed mostly spherical particles in the size range of 5 nm–25 nm. (B) XRD pattern of the OA-synthesized AgNPs using *O. arabicus* extract showing the facets of crystalline silver.

were spherical with the average diameter ranging from 5 nm to 25 nm (Fig. 2A). The darker shaded capping on the NP surface showed the presence of secondary materials that may be attributed to bio-compounds present in the *O. arabicus* leaves extract. These bio-components can reduce the efficiency of Ag salts in NPs and serve as suitable capping agents to prevent aggregation of NPs (Makarov et al., 2014).

3.2. Cytotoxicity of OA-synthesized AgNPs

The cytotoxicity of the OA-synthesized AgNPs in MCF-7 cells at various concentrations (15 μg/mL, 25 μg/mL, 50 μg/mL, 100 μg/mL, 200 μg/mL, 300 μg/mL, 400 μg/mL, 500 μg/mL, and 600 μg/mL) was evaluated by the MTT assay. The percentage cell viability was found to be 9.95% and 88.54% at the highest (600 μg/mL) and lowest (15 μg/mL) concentration of the OA-synthesized AgNPs (Fig. 3), respectively, indicating a visible dose-dependent effect of the OA-synthesized AgNPs. The IC_{50} value of the OA-synthesized AgNPs was estimated at 100 μg/mL. Based on these findings, three different sub-lethal concentrations (25 μg/mL, 50 μg/mL, and 75 μg/mL) of the OA-synthesized AgNPs were subsequently used in the experiments. Further, the morphology of the MCF-7 cells treated with OA-synthesized AgNPs for 24 h was examined under inverted microscopy. Control cells displayed a normal morphology (Fig. 4 control); the cells attached to the surface and attained a growth of about 96%–100%. Cell death was evidently observed in the OA-synthesized AgNPs treated MCF-7 cells. Additionally, cell

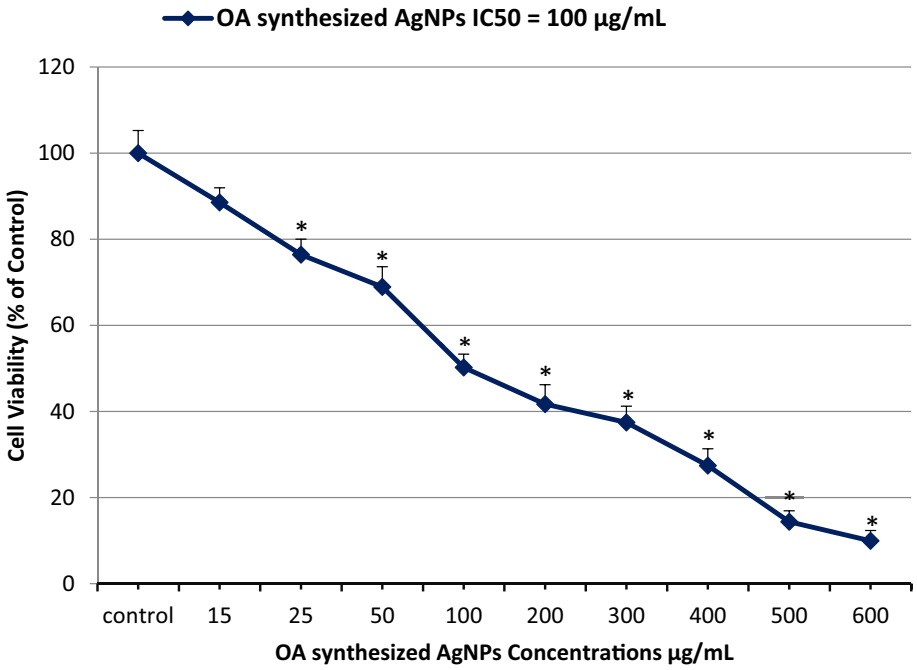

Fig. 3. Inhibition of MCF-7 cell proliferation after treatment of the cells with the indicated concentrations of OA-synthesized AgNPs. The IC_{50} value post 24 h of exposure was estimated to be 100 µg/mL by the MTT assay.

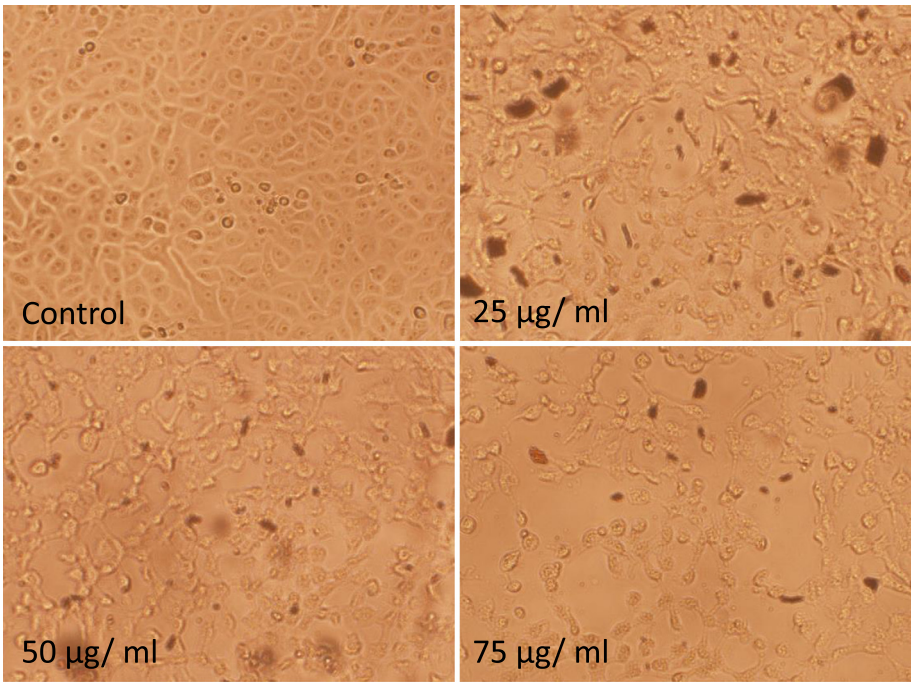

Fig. 4. Morphological changes in MCF-7 cells after exposure of the cells to the indicated concentrations of OA-synthesized AgNPs for 24 h. The untreated cells (control) were normal in terms of growth and shape. The treated cells exhibited loss of cell adhesion and decreased cell density due to cell death (25 µg/mL–75 µg/mL) (magnification 100X).

shrinkage was evident with the loss of cell adhesion, reduced cell size, and decreased cell density (Fig. 4 25–75 µg/mL).

3.3. Intracellular ROS measurement

The intracellular ROS generation in MCF-7 cells was evaluated by DCFH-DA fluorescence staining. Fig. 5A-5D display representative fluorescence images obtained after the exposure of the cells to the OA-synthesized AgNPs for 24 h. A concentration-dependent elevation in the ROS level was observed in the exposed cells compared to that in control. The pattern of increased intensity of green fluorescence was also confirmed by quantitative estimation, where a significant ($p < 0.05$) increase in the ROS level (123%, 165%, and 191%) was observed in the cells treated with 25 µg/mL, 50 µg/mL, and 75 µg/mL OA-synthesized AgNPs compared to that in the control cells (Fig. 5E).

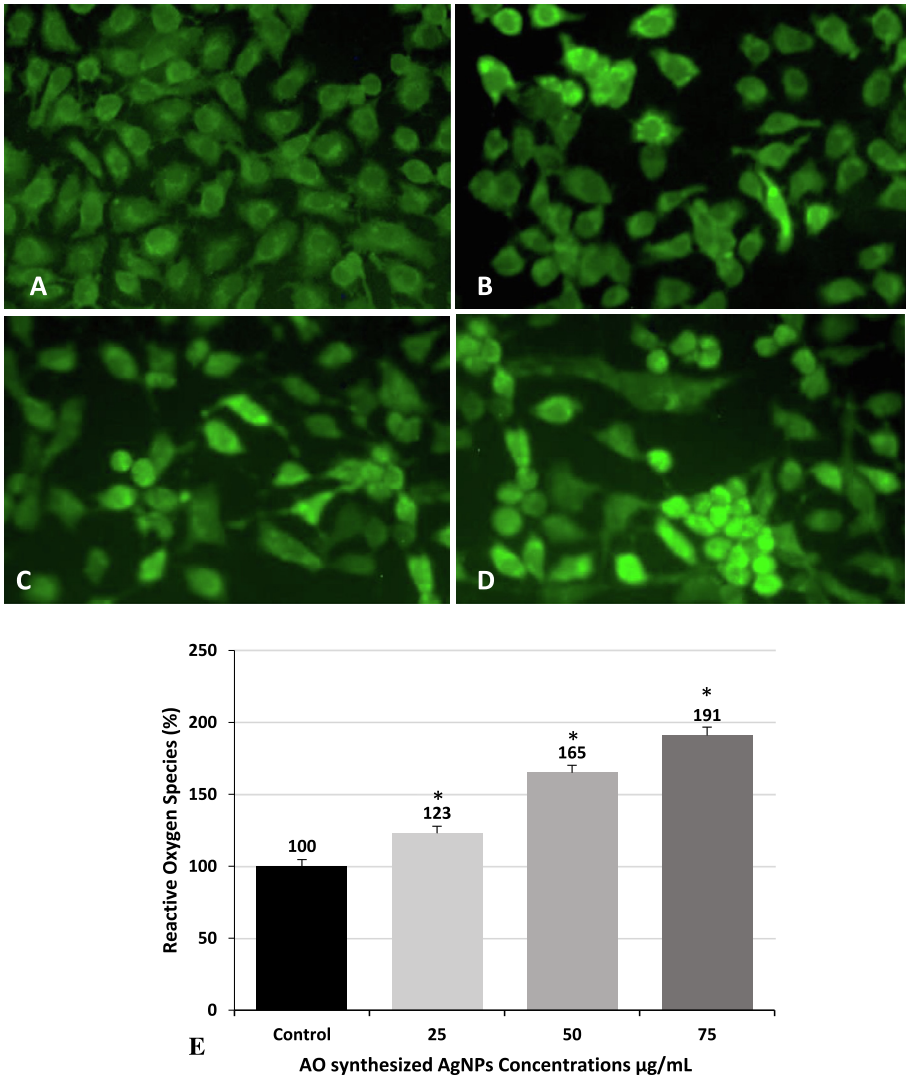

Fig. 5. Detection of intracellular ROS induced by OA-synthesized AgNPs in MCF-7 cells by fluorescence microscopy. (A) Control cells, (B) 25 µg/mL (C) 50 µg/mL, and (D) 75 µg/mL. (E) Detection of intracellular ROS by measurement of fluorescent intensity. The values have been expressed as mean ± SE (*Significant, $p < 0.05$).

3.4. Annexin-V apoptosis assay

The extent of apoptosis in MCF-7 cells was quantified as shown in the representative dot plots; 1.75%, 1.62%, and 0.58% of the untreated cells underwent early apoptosis, late apoptosis, and necrosis, respectively. The incidence of apoptosis in the control group reflected the natural course of these events during cell growth in culture. Treatment with 25, 50, and 75 µg/mL OA-synthesized AgNPs significantly ($p < 0.05$) increased the proportion of cells that underwent early apoptosis (5.38%, 6.55%, and 8.35%, respectively), late apoptosis (12.59%, 14.51%, and 17.32%, respectively), and necrosis (11.38%, 11.68%, and 14.65%, respectively) compared to that in the control cells post 24 h of exposure (Fig. 6A–D).

3.5. Detection of apoptotic changes in MCF-7 cells

To analyze whether the increase in cell death was due to apoptosis, the MCF-7 cells were exposed to OA-synthesized AgNPs as indicated above (Section 3.2) for 24 h and stained with AO and ethidium bromide. About 92.2% of viable cells were observed among the untreated MCF-7 cells. These cells showed even distribution of the AO stain (green fluorescence) with normal nuclear morphology and no red fluorescence (Fig. 7A). A significant ($p < 0.05$) decrease in the percentage of viable cells was registered in all the treated samples. Conversely, the percentage of apoptotic cells increased significantly in all the treatments as seen by the number of red-colored cells (Fig. 7B-7D). In each group, 300 cells were analyzed for quantifying the apoptotic and necrotic cells, which revealed that OA-synthesized AgNPs induced the highest percentage of apoptotic (26%) and necrotic (12%) cells at the highest concentration of 75 µg/mL (Fig. 7E).

3.6. Detection of autophagy by acridine orange staining

To elucidate the role of OA-synthesized AgNPs in inducing autophagy in the MCF-7 cells, AO dye was used for the detection of acidic vesicular organelles (AVOs). Treatment of MCF-7 cells with OA-synthesized AgNPs (25 µg/mL, 50 µg/mL, and 75 µg/mL) for 24 h revealed the appearance of AVOs. Images obtained from fluorescence microscopy revealed that the control MCF-7 cells exhibited minimum number of AVOs in the cytoplasm and showed mostly green fluorescence with minimal red/orange fluorescence (Fig. 8A). Conversely, comparatively more number of AVOs was

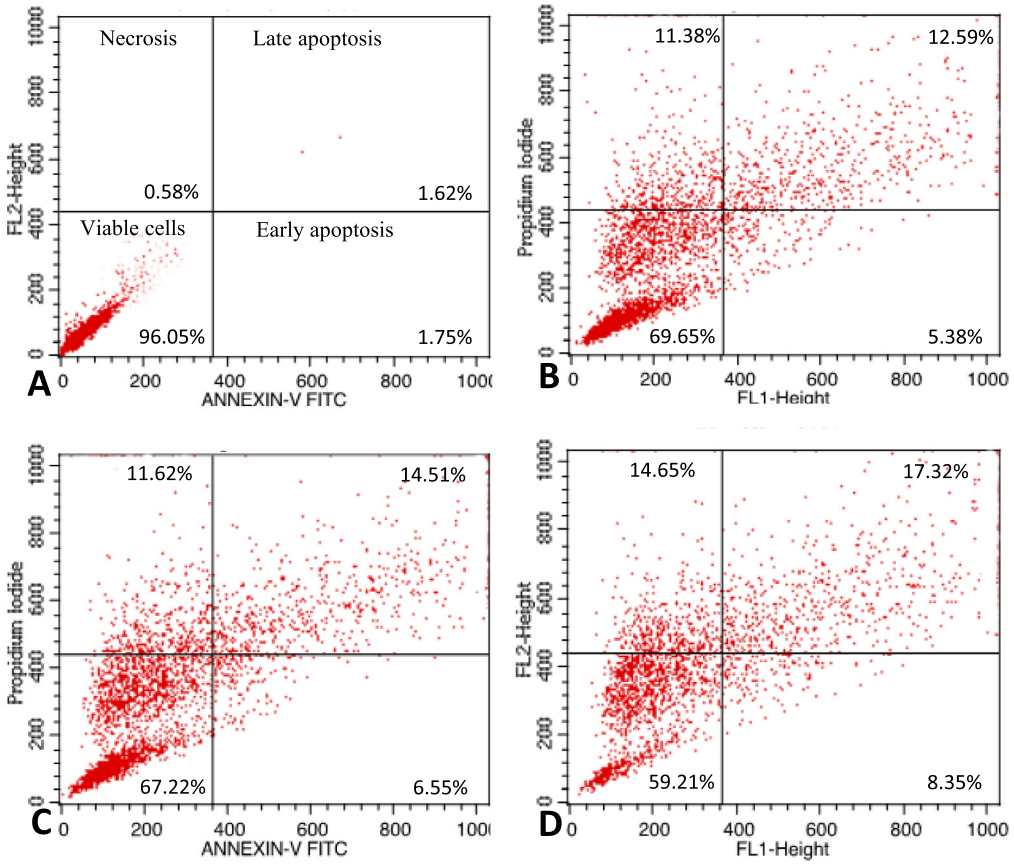

Fig. 6. Detection of apoptosis in MCF-7 cells by annexin V-FITC/PI staining analyzed by flow cytometry. The percentage of viable cells and of cells undergoing early apoptosis, late apoptosis, and necrosis has been shown. (A) Control cells, (B) cells treated with 25 μg/mL OA-synthesized AgNPs, (C) cells treated with 50 μg/mL OA-synthesized AgNPs, and (D) cells treated with 75 μg/mL OA-synthesized AgNPs.

observed in the perinuclear region of the cytoplasm in majority of the treated cells (Fig. 8B–D).

4. Discussion

AgNPs biosynthesized from medicinal plant extracts, including OA-synthesized AgNPs, may play critical roles in refining the compatibility and bioavailability of natural products in the treatment of several chronic diseases. Analysis of the UV–vis spectrum provides valuable information for structurally characterizing AgNPs. Due to the presence of capping agent, the absorbance of AgNPs is governed mainly by their shape and size (Sherry et al., 2005). In general, SPR peaks decrease in number as the symmetry of the NPs increases (Nehl et al., 2006).

The exact mechanism of the biosynthesis of AgNPs using leaf extracts of plants remains unclear, but may involve chemical constituents such as phenolics, proteins, and reducing agents (Satyavani et al., 2011). The stabilization and reduction of Ag+ by a combination of biomolecules found in the leaves extracts of plants, including proteins, enzymes, amino acids, polysaccharides, alkaloids, phenolics, saponins, tannins, vitamins, and terpenoids, has been documented (Kulkarni and Muddapur, 2014; Benelli, 2016). Biosynthesis of AgNPs involves organic molecules functioning as capping agents that help in stabilizing the NPs (Benelli, 2016). The results of current study further corroborated the OA-synthesized AgNPs synthesis as sharp bands typical of the Bragg peaks were observed in X-ray diffraction, which may be due to the various reducing agents present in the *O. arabicus* leaves extract (Balakrishnan et al., 2016). The biologically active biocomponents of leaves extracts and Ag salts are diverse in terms of concentration and bio-composition. The variation in the reaction conditions and composition of a reaction mixture through changes in pH and temperature and inclusion of bio-matrices as additives serves to control the morphology, shape, and size of NPs (Ahmed et al., 2016).

In a previous study using a crude ethanolic extract of *O. arabicus*, the IC_{50} value in MCF-7 cells was determined to be 562 μg/mL (Ali et al., 2016). Conversely, the IC_{50} value of the MCF-7 cells treated with pure AgNPs was found to be 73 μg/mL (Farah et al., 2016). The cytotoxic effect of OA-synthesized AgNPs may be attributed to the high content of flavonoid glycosides found in *O. arabicus*, which may be involved in the reduction process of OA-synthesized AgNPs. Phytochemical investigations of plants of the family *Resedaceae*, including *Caylusea, Ochradenus, and Reseda*, revealed the presence of various flavonoid glycosides, including kaempferol, isorhamnetin, luteolin, and quercetin (Villelaet al., 2011; Ali et al., 2016). These flavonoid glycosides may have antineoplastic properties and a potent ability to induce cell death via molecular mechanisms that include activation of the intrinsic pathway of autophagy, generation of ROS, and apoptosis (Wu et al., 2016). Apoptosis has been identified as a major mechanism of death in cells exposed to AgNPs synthesized using a plant extract (Farah et al., 2016). However, additional parameters may be operative in the NP-induced cell death (Khan et al., 2007).

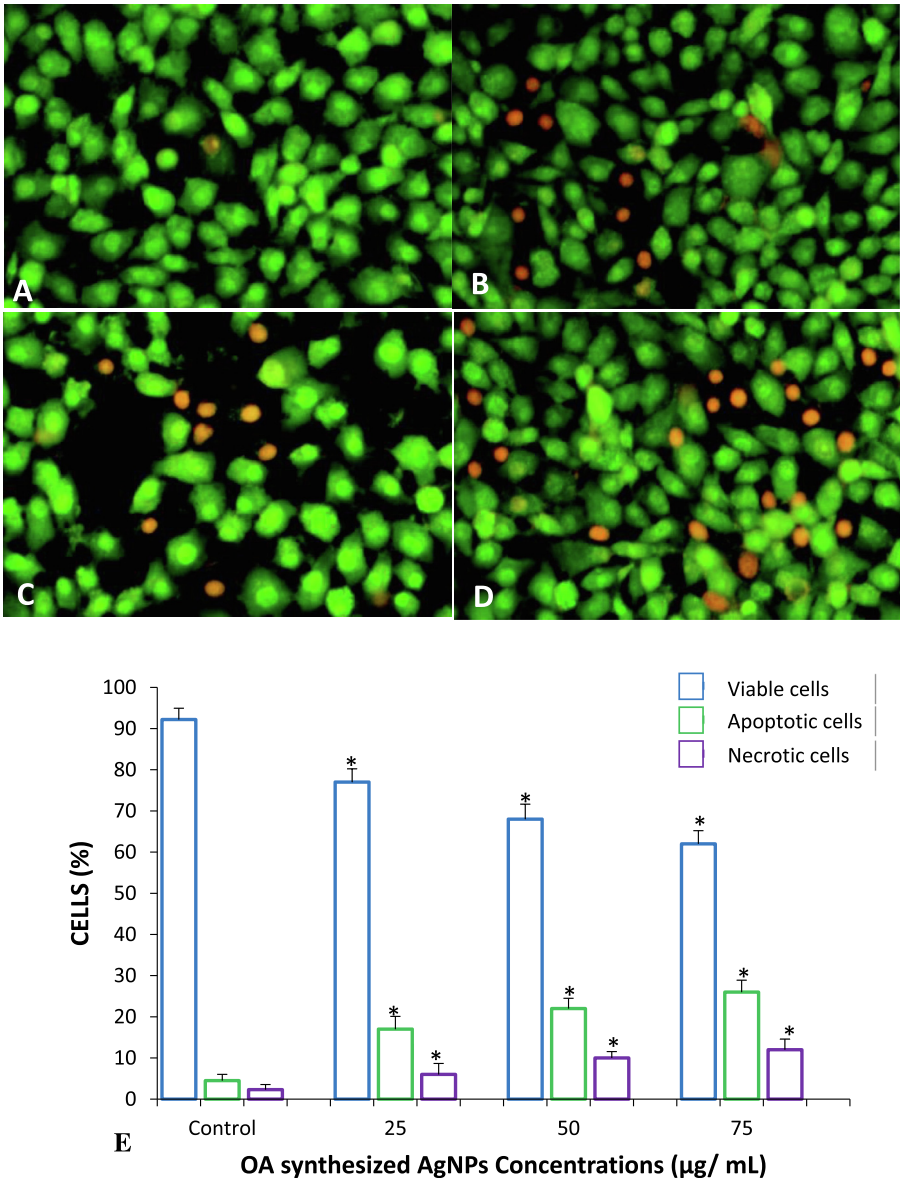

Fig. 7. Dual staining of MCF-7 cells with acridine orange and ethidium bromide for the analysis of apoptotic morphological changes induced by OA-synthesized AgNPs observed under fluorescence microscopy. (A) Control cells, (B) 25 µg/mL (C) 50 µg/mL (D) 75 µg/mL. Magnification: 200×. (E) Quantification of apoptotic and necrotic cells based on the uptake of acridine orange and ethidium bromide (number of cells analyzed in each group = 300). All data have been expressed as mean ± SE. * Significant ($p < 0.05$) compared with corresponding controls.

The interaction between AgNPs and mammalian cells can lead to induction of oxidative stress through production of ROS at a concentration that can eliminate antioxidants, such as reduced glutathione, and inhibit antioxidant enzymes, including superoxide dismutase and glutathione peroxidase, which results in DNA damage (Asharani et al., 2009; Foldbjerg et al., 2011). Induction of oxidative stress is one of the important mechanisms of toxicity of AgNPs (Gurunathan et al., 2013). Increased intracellular ROS causes oxidative damage to cell components, which ultimately leads to cell death (Mohamed et al., 2014). Oxidative stress can promote apoptosis in response to a variety of signals and pathophysiological situations (Foldbjerg et al., 2011). It has been reported that AgNPs synthesized from the extract of leaves can induce oxidative stress (Farah et al., 2016). Hence, intracellular ROS can be a crucial indicator of the toxic effects of NPs (Suliman et al., 2015).

A relationship has been documented between autophagy and ROS, where the generation of ROS eventually leads to apoptosis and autophagy (Vlahakis et al., 2017; Smuder et al., 2018). Therefore, in this study, we sought to understand and clarify the roles of autophagy and ROS in determining the fate of the MCF-7 breast cancer cells treated with OA-synthesized AgNPs. Lee et al. (2014) suggested that the cells exposed to excess ROS because of treatment with AgNPs may undergo altered autophagy, which results in the accumulation of damage to organelles like mitochondria, which can induce inflammation, DNA damage, and oxidative stress. The results obtained in this study were found to be consistent with previous reports (Farah et al., 2016; Buttacavoli et al., 2018). Dysfunction in the autophagy process has been recognized as a possible mechanism of cell death, resulting in either autophagy or apoptosis (Kroemer and Jäättelä, 2005). The metabolic rate in all types of cancer cells is higher than the basal rate, which results in an increased level of intracellular ROS (Buttacavoli et al., 2018) that ultimately leads to increase in oxidative stress in the cells, making them more vulnerable to an ROS-mediated attack and, eventually, cell death (Ling et al., 2011). ROS selectively targets

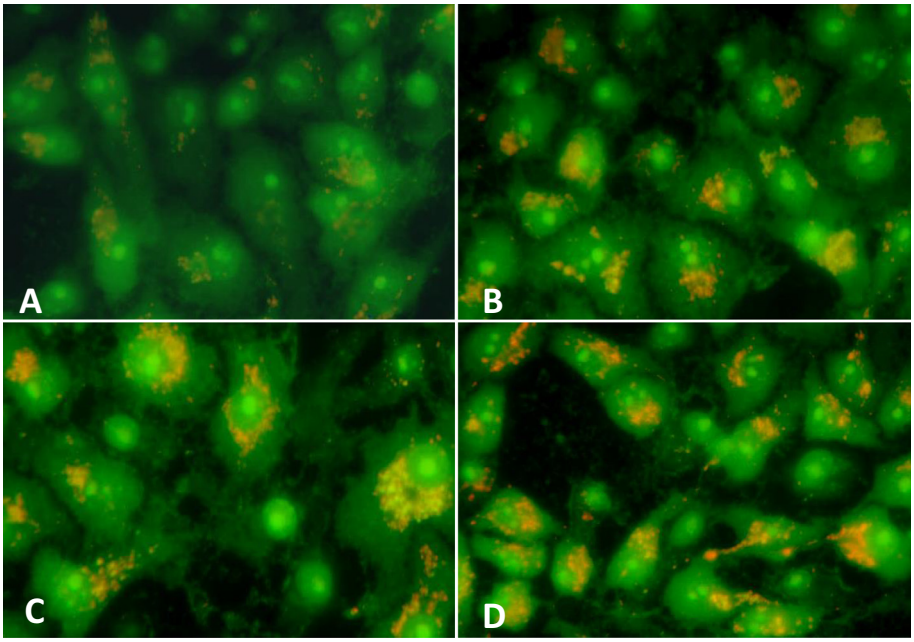

Fig. 8. Induction of autophagy in MCF-7 cells was evaluated based on the formation of acidic vesicular organelles (AVOs) stained by acridine orange. The cells were exposed to OA-synthesized AgNPs for 24 h (A) Control cells, (B) 25 μg/mL (C) 50 μg/mL (D) 75 μg/mL. Magnification: 400X.

malignant cancer cells for the induction of autophagy, which has significant effects on anticancer therapy, including breast cancer. The role of autophagy in apoptosis is important because of the potential of autophagy in modifying cell death. Thus, autophagy has been considered a therapeutic target in neurodegeneration and cancer (Ling et al., 2011; Kim et al., 2019).

5. Conclusions

The present study demonstrated the potential of medicinal plant *O. arabicus* as a capping and biological reducing agent for the synthesis of new materials. OA-synthesized AgNPs can be synthesized easily, rapidly, and inexpensively. The viability of MCF-7 cells treated with various concentrations of OA-synthesized AgNPs was decreased in a dose-dependent manner. The IC_{50} value of the OA-synthesized AgNPs (100 μg/mL) was found to be decreased compared to that of the crude extract. OA-synthesized AgNPs also increased the intracellular ROS levels and enhanced the rate of autophagy and apoptosis. These results suggest that biocompatibility of AgNPs was increased as its toxicity was reduced as compared to pure AgNPs. The phytochemicals from *O. arabicus* increases the anticancer activities of crude extract when used as reducing agent for AgNPs synthesis. Owing to their enhanced bioavailability and compatibility, biosynthesized AgNPs have a high potential for use in therapeutic applications for chronic diseases, including cancer.

Declaration of Competing Interest

The authors declare that they have no known competing financial interests or personal relationships that could have appeared to influence the work reported in this paper.

Acknowledgments

The authors would like to thank the Deanship of scientific research for funding and supporting this research through the initiative of the DSR Graduate Students Research Support (GSR). The authors thank the Deanship of Scientific Research and RSSU at King Saud University for their technical support.

References

Ahmed, S., Ahmad, M., Swami, B.L., Ikram, S., 2016. A review on plants extract mediated synthesis of silver nanoparticles for antimicrobial applications: a green expertise. J. Adv. Res. 7 (1), 17–28. https://doi.org/10.1016/j.jare.2015.02.007.

Ali, M.A., Farah, M.A., Al-Hemaid, F.M., Abou-Tarboush, F.M., Al-Anazi, K.M., Wabaidur, S.M., Alothman, Z.A., Lee, J., 2016. Assessment of biological activity and UPLC–MS based chromatographic profiling of ethanolic extract of *Ochradenus arabicus*. Saudi J. Biol. Sci. 23 (2), 229–236. https://doi.org/10.1016/j.sjbs.2015.02.010.

Arulvasu, C., Prabhu, D., Manikandan, R., Srinivasan, P., Dinesh, D., Babu, G., Sellamuthu, P., 2010. Induction of apoptosis by the aqueous and ethanolic leaf extract of *Vitex negundo L.* in MCF-7 human breast cancer cells. Int. J. Drug. Discov. 2, 1–7. https://doi.org/10.9735/0975-4423.2.1.1-7.

Asharani, P.V., Hande, M.P., Valiyaveettil, S., 2009. Anti-proliferative activity of silver nanoparticles. BMC Cell Biol. 10 (1), 65–79. https://doi.org/10.1186/1471-2121-10-65.

Balakrishnan, S., Srinivasan, M., Mohanraj, J., 2016. Biosynthesis of silver nanoparticles from mangrove plant (*Avicennia marina*) extract and their potential mosquito larvicidal property. J. Parasit. Dis. 40 (3), 991–996. https://doi.org/10.1007/s12639-014-0621-5.

Benelli, G., 2016. Plant-mediated biosynthesis of nanoparticles as an emerging tool against mosquitoes of medical and veterinary importance: a review. Parasitol. Res. 115 (1), 23–34. https://doi.org/10.1007/s00436-015-4800-9.

Buttacavoli, M., Albanese, N.N., Di Cara, G., Alduina, R., Faleri, C., Gallo, M., Pizzolanti, G., Gallo, G., Feo, S., Baldi, F., Cancemi, P., 2018. Anticancer activity of biogenerated silver nanoparticles: an integrated proteomic investigation. Oncotarget 9 (11), 9685–9705. https://doi.org/10.18632/oncotarget.23859.

Deavall, D.G., Martin, E.A., Horner, J.M., Roberts, R., 2012. Drug-induced oxidative stress and toxicity. J. Toxicol. 10, 645–1460. https://doi.org/10.1155/2012/645460.

Dwivedi, A.D., Gopal, K., 2010. Biosynthesis of silver and gold nanoparticles using *Chenopodium album* leaf extract. Colloids Surf. A Physicochem. Eng. Asp. 369, 27–33. https://doi.org/10.1016/j.colsurfa.2010.07.020.

Farah, M.A., Ali, M.A., Chen, S.M., Li, Y., Al-Hemaid, F.M., Abou-Tarboush, F.M., Al-Anazi, K.M., Lee, J., 2016. Silver nanoparticles synthesized from *Adenium obesum* leaf extract induced DNA damage, apoptosis and autophagy via generation of reactive oxygen species. Colloids Surf. B. Biointerfaces. 141, 158–169. https://doi.org/10.1016/j.colsurfb.2016.01.027.

Foldbjerg, R., Dang, D.A., Autrup, H., 2011. Cytotoxicity and genotoxicity of silver nanoparticles in the human lung cancer cell line, A549. Arch. Toxicol. 85 (7), 743–750. https://doi.org/10.1007/s00204-010-0545-5.

Ghaffari-Moghaddam, M., Hadi-Dabanlou, R., Khajeh, M., Rakhshanipour, M., Shameli, K., 2014. Green synthesis of silver nanoparticles using plant extracts. Korean J. Chem. Eng. 4, 548–557. https://doi.org/10.1007/s11814-014-0014-6.

Gurunathan, S., Raman, J., Abd Malek, S.N., John, P.A., Vikineswary, S., 2013. Green synthesis of silver nanoparticles using *Ganoderma neo-japonicum* Imazeki: a potential cytotoxic agent against breast cancer cells. Int. J. Nanomedicine 8 (1), 4399–4413. https://doi.org/10.2147/IJN.S51881.

Jemal, A., Bray, F., Ferlay, J., Ward, E., Forman, D., 2011. Global cancer statistics. CA Cancer J. Clin. 61, 69–90. https://doi.org/10.3322/caac.20107.

Khan, J.A., Pillai, B., Das, T.K., Singh, Y., Maiti, S., 2007. Molecular effects of uptake of gold nanoparticles in HeLa cells. ChemBioChem 8 (11), 1237–1240. https://doi.org/10.1002/cbic.200700165.

Kim, Y.J., Rahman, M.M., Lee, S.M., Kim, J.M., Park, K., Kang, J.H., Seo, Y.R., 2019. Assessment of in vivo genotoxicity of citrated-coated silver nanoparticles via transcriptomic analysis of rabbit liver tissue. Int. J. Nanomed. 14, 393–405. https://doi.org/10.2147/IJN.S174515.

Kroemer, G., Jäättelä, M., 2005. Lysosomes and autophagy in cell death control. Nat. Rev. Cancer. 5 (11), 886–897. https://doi.org/10.1038/nrc1738.

Kulkarni, N., Muddapur, U., 2014. Biosynthesis of metal nanoparticles: a review. J. Nanotechnol. 2014, 1–8. https://doi.org/10.1155/2014/510246.

Kuppusamy, P., Yusoff, M.M., Maniam, G.P., Govindan, N., 2016. Biosynthesis of metallic nanoparticles using plant derivatives and their new avenues in pharmacological applications – an updated report. Saudi Pharm. J. 24 (4), 473–484. https://doi.org/10.1016/j.jsps.2014.11.013.

Lee, Y.H., Cheng, F.Y., Chiu, H.W., Tsai, J.C., Fang, C.Y., Chen, C.W., Wang, Y.J., 2014. Cytotoxicity, oxidative stress, apoptosis and the autophagic effects of silver nanoparticles in mouse embryonic fibroblasts. Biomaterials 35 (16), 4706–4715. https://doi.org/10.1016/j.biomaterials.2014.02.021.

Ling, L.U., Tan, K.B., Lin, H., Chiu, G.N.C., 2011. The role of reactive oxygen species and autophagy in safingol-induced cell death. Cell Death Dis. 2, (3). https://doi.org/10.1038/cddis.2011.12 e129.

Lodha, R.S., Nandeshwar, S., Pal, D.K., Shrivastav, A., Lodha, K.M., Bhagat, V.K., Bankwar, V., Saxena, D.M., 2011. Risk factors for breast cancer among women in Bhopal urban agglomerate: a case control study. Asian Pac. J. Cancer Prev. 12, 2111–2115.

Makarov, V.V., Love, A.J., Sinitsyna, O.V., Makarova, S.S., Yaminsky, I.V., Taliansky, M. E., Kalinina, N.O., 2014. "Green" nanotechnologies: synthesis of metal nanoparticles using plants. Acta. Natur. 6 (1), 35–44. https://doi.org/10.32607/20758251-2014-6-1-35-44.

Miller, A.G., 1984. A revision of Ochradenus. Notes Roy. Bot. Gard. Edinburgh 41, 491–594.

Mohamed, N.H., Ismail, M.A., Abdel-Mageed, W.M., Shoreit, A.A.M., 2014. Antimicrobial activity of latex silver nanoparticles using *Calotropis procera*. Asian Pac. J. Trop. Biomed. 4 (11), 876–883. https://doi.org/10.12980/APJTB.4.201414B216.

Mosmann, T., 1983. Rapid colorimetric assay for cellular growth and survival: application to proliferation and cytotoxicity assays. J. Immunol. Methods 65 (1–2), 55–63. https://doi.org/10.1016/0022-1759(83)90303-4.

Nehl, C.L., Liao, H., Hafner, J.H., 2006. Optical properties of star-shaped gold nanoparticles. Nano Lett. 6 (4), 683–688. https://doi.org/10.1021/nl052409y.

Nel, A., Xia, T., Mädler, L., Li, N., 2006. Toxic potential of materials at the nanolevel. Science 311, 622–627. https://doi.org/10.1126/science.1114397.

Rao, P.V., Nallappan, D., Madhavi, K., Rahman, S., Jun Wei, L., Gan, S.H., 2016. Phytochemicals and biogenic metallic nanoparticles as anticancer agents. Oxid. Med. 2016, 1–15. https://doi.org/10.1155/2016/3685671.

Ribeiro, F., Gallego-Urrea, J.A., Jurkschat, K., Crossley, A., Hassellöv, M., Taylor, C., Soares, A.M., Loureiro, S., 2013. Silver nanoparticles and silver nitrate induce high toxicity to *Pseudokirchneriella subcapitata, Daphnia magna* and *Danio rerio*. Sci. Total Environ. 466, 232–241. https://doi.org/10.1016/j.scitotenv.2013.06.101.

Rodriguez-Rocha, H., Garcia-Garcia, A., Panayiotidis, M.I., Franco, R., 2011. DNA damage and autophagy. Mutat. Res. 711, 158–166. https://doi.org/10.1016/j.mrfmmm.2011.03.007.

Satyavani, K., Gurudeeban, S., Ramanathan, T., Balasubramanian, T., 2011. Biomedical potential of silver nanoparticles synthesized from calli cells of *Citrullus colocynthis* (L.). Schrad. J. Nanobiotech. 9 (1), 43–51. https://doi.org/10.1186/1477-3155-9-43.

Sherry, L.J., Chang, S.H., Schatz, G.C., Van Duyne, R.P., Wiley, B.J., Xia, Y., 2005. Localized surface plasmon resonance spectroscopy of single silver nanocubes. Nano Lett. 5 (10), 2034–2038. https://doi.org/10.1021/nl0515753.

Smuder, A.J., Sollanek, K.J., Nelson, W.B., Min, K., Talbert, E.E., Kavazis, A.N., Hudson, M.B., Sandri, M., Szeto, H.H., Powers, S.K., 2018. Crosstalk between autophagy and oxidative stress regulates proteolysis in the diaphragm during mechanical ventilation. Free Radic. Biol. Med. 115, 179–190. https://doi.org/10.1016/j.freeradbiomed.2017.11.025.

Suliman, Y.A.O., Ali, D., Alarifi, S., Harrath, A.H., Mansour, L., Alwasel, S.H., 2015. Evaluation of cytotoxic, oxidative stress, proinflammatory and genotoxic effect of silver nanoparticles in human lung epithelial cells. Environ. Toxicol. 30 (2), 149–160. https://doi.org/10.1002/tox.21880.

Villela, A., van der Klift, E.J., Mattheussens, E.S., Derksen, G.C., Zuilhof, H., van Beek, T.A., 2011. Fast chromatographic separation for the quantitation of the main flavone dyes in *Reseda luteola* (weld). J. Chromatogr. A 1218 (47), 8544–8550. https://doi.org/10.1016/j.chroma.2011.09.069.

Vlahakis, A., Lopez Muniozguren, N., Powers, T., 2017. Stress-response transcription factors Msn2 and Msn4 couple TORC2-Ypk1 signaling and mitochondrial respiration to ATG8 gene expression and autophagy. Autophagy 13 (11), 1804–1812. https://doi.org/10.1080/15548627.2017.1356949.

Wu, H., Lin, J., Liu, P., Huang, Z., Zhao, P., Jin, H., Ma, J., Wen, L., Gu, N., 2016. Reactive oxygen species acts as executor in radiation enhancement and autophagy inducing by AgNPs. Biomaterials 101, 1–9. https://doi.org/10.1016/j.biomaterials.2016.05.031.